ACS APPLIED MATERIALS & INTERFACES

Research Article

www.acsami.org

Facile Synthesis of Lithium Sulfide Nanocrystals for Use in Advanced Rechargeable Batteries

Xuemin Li,[†] Colin A. Wolden,*[,‡] Chunmei Ban,[§] and Yongan Yang*[,†]

[†]Department of Chemistry, Colorado School of Mines, 1012 14th Street, Golden, Colorado 80401, United States

[‡]Department of Chemical and Biological Engineering, Colorado School of Mines, 1613 Illinois Street, Golden, Colorado 80401, United States

[§]National Renewable Energy Laboratory, 1617 Cole Boulevard, Golden, Colorado 80401, United States

Supporting Information

ABSTRACT: This work reports a new method of synthesizing anhydrous lithium sulfide (Li_2S) nanocrystals and demonstrates their potential as cathode materials for advanced rechargeable batteries. Li_2S is synthesized by reacting hydrogen sulfide (H_2S) with lithium naphthalenide (Li-NAP), a thermodynamically spontaneous reaction that proceeds to completion rapidly at ambient temperature and pressure. The process completely removes H_2S, a major industrial waste, while cogenerating 1,4-dihydronaphthalene, itself a value-added chemical that can be used as liquid fuel. The phase purity, morphology, and homogeneity of the resulting nanopowders were confirmed by X-ray diffraction and scanning electron microscopy. The synthesized Li_2S nanoparticles (100 nm) were assembled into cathodes, and their performance was compared to that of cathodes fabricated using commercial Li_2S micropowders (1−5 μm). Electrochemical analyses demonstrated that the synthesized Li_2S were superior in terms of (dis)charge capacity, cycling stability, output voltage, and voltage efficiency.

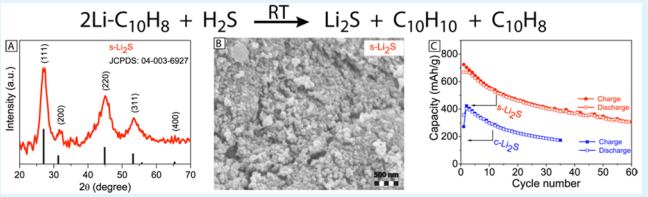

KEYWORDS: *lithium sulfide, lithium−sulfur batteries, synthesis, hydrogen sulfide, lithium naphthalenide*

1. INTRODUCTION

Rechargeable batteries are ubiquitous power sources in our modern society. Their applications span from personal devices to national defense, from chemical sensors to human health, and from ground transportation to spacecrafts.[1−3] Currently, the most advanced rechargeable batteries are lithium-ion batteries (LIBs, which typically employ graphite anodes and lithium−cobalt oxide cathodes).[4] While they are superior to conventional counterparts (such as nickel−cadmium batteries), more advanced LIBs and beyond-lithium technologies with higher specific energy (energy per unit mass), higher energy density (energy per unit volume), lower cost, and safer chemistry/fabrication are imperative to meet the demand of sustainable development.[4]

Lithium−sulfur (Li−S) batteries are widely considered the most promising power sources in the near future for developing more advanced portable devices, electric vehicles, and stationary energy-storage facilities.[5] Compared with the current-generation LIBs, Li−S batteries hold two remarkable advantages:[5,6] (1) presenting higher specific energy (2600 vs 580 Wh/kg) and energy density (2200 vs 1800 Wh/L); (2) using earth-abundant and cost-effective materials in the cathode (S vs Co). However, the direct use of a lithium metal anode and a sulfur cathode ensues some challenges.[7−9] First, cycling can lead to the formation of harmful dendrites on the lithium metal anode, which can grow and penetrate the separator, potentially causing short-circuit, thermal runaway, and even severe fire.[8,10] Second, it is difficult to engineer the sulfur cathode to provide sufficient void space to accommodate the 80% volume expansion that accompanies lithiation, which often pulverizes the electrode and damages the electrical contact.[8] An alternative approach that avoids these problems is to use lithium sulfide (Li_2S) as the cathode.[11]

While Li_2S and sulfur are both poor electronic and ionic conductors, which would typically preclude their use in electrochemical applications, Li_2S presents several advantages.[11] First, the use of Li_2S avoids the problems associated with lithium metal anodes, and it can directly be paired with existing anode materials (graphite) as well as new lithium-free materials (such as silicon and tin) for assembling batteries.[12] The practical specific energy of Li_2S−Si (930 Wh/kg) is close to that of a Li−S battery (1000 Wh/kg).[9] Second, because of its much higher melting/boiling points, Li_2S permits a wider temperature window for electrode fabrication.[4] Third, Li_2S is fully lithiated, not a requiring preset void space around Li_2S particles for accommodating the detrimental volume fluctuations that occur during the charge/discharge cycles.[13,14] Fourth, although a dry room or glovebox is required for electrode fabrication,[9] Li_2S allows batteries to be assembled in the "discharged" state, a safer and more cost-effective process.[8]

Received: October 3, 2015
Accepted: December 3, 2015
Published: December 3, 2015

DOI: 10.1021/acsami.5b09367
ACS Appl. Mater. Interfaces 2015, 7, 28444−28451

Moreover, recently, scientists showed that the issues of poor electronic and ionic conductivity for Li_2S could be overcome by either applying a high activation potential or using nanoparticles.[4,9,15] Therefore, Li_2S nanoparticles are highly desirable for developing Li−S batteries; a large demand is expected in the near future.

However, commercially, Li_2S is only available as micropowders, reflecting high-temperature processes used for industrial synthesis.[16,17] The primary techniques are[16−19]

$$2Li + S \xrightarrow{T\geq 300^\circ C} Li_2S \qquad \Delta G_m^\circ(Li_2S) \approx -414\ kJ/mol \tag{1}$$

$$Li_2SO_4 + 2C \xrightarrow{T=600-1000^\circ C} Li_2S + 2CO_2$$
$$\Delta G_m^\circ(Li_2S) \approx +119\ kJ/mol \tag{2}$$

$$Li_2CO_3 + H_2S \xrightarrow{T=600-1000^\circ C} Li_2S + H_2O + CO_2$$
$$\Delta G_m^\circ(Li_2S) \approx +120\ kJ/mol \tag{3}$$

Because lithium and sulfur both are very reactive at elevated temperatures, the operation of reaction (1) is challenging, although it is a thermodynamically favorable reaction. An alternative way of running reaction (1) is to dissolve lithium in liquid NH_3 at <−33 °C, but this approach brings additional complications. Reactions (2) and (3) are endothermic carbothermal reduction processes that require high temperatures and produce greenhouse gas. In addition, product purification in these three methods is also expected to be complicated and costly because at least one reactant is in the same phase as Li_2S.

Another drawback of current approaches is the size of the resulting powders (1−10 μm). It is commonly reported in the battery literature that nanostructured materials are superior to their bulk counterparts.[11] Large surface/volume ratios promote thorough lithiation/delithiation [high (dis)charge capacity], fast diffusion (high rate capability), and mechanical resilience (high cycling stability).[11] Current approaches to convert Li_2S micropowders into nanocrystals include ball milling[9,20−24] and recrystallization of dissolved Li_2S,[4,25−28] but these approaches are both energy-intensive and time-consuming. A more elegant strategy would be the direct synthesis of Li_2S nanocrystals. One approach being pursued is chemical/electrochemical lithiation of sulfur nanoparticles,[12,15,29−31] but this multistep process requires synthesis of well-dispersed sulfur nanoparticles. Recently, two research groups reported direct syntheses of Li_2S nanocrystals by reacting lithium sulfate with carbon precursors at high temperatures (820−900 °C) for >2 h.[32,33] Elam et al. synthesized amorphous Li_2S nanofilms using a vapor-phase atomic layer deposition via alternating exposure to lithium *tert*-butoxide and hydrogen sulfide.[34] However, it seems challenging for these methods to produce Li_2S nanocrystals at large scale.

This work reports a scalable, high-throughput, room temperature approach to synthesizing Li_2S nanocrystals, by reacting hydrogen sulfide (H_2S) with lithium naphthalenide (Li-NAP), a thermodynamically spontaneous reaction that proceeds to completion rapidly at ambient pressure. The simple reaction directly generates Li_2S nanocrystals that precipitate out of solution, allowing easy recovery and purification. Because the value of Li_2S is many times higher than that of lithium, the cost of lithium seems less likely to be a limiting factor for industrial production. Furthermore, ancillary benefits of this reaction include the removal of H_2S, a hazardous waste requiring abatement, and the production of 1,4-dihydronaphthalene, itself a value-added product with applications as an industrial solvent and a fuel additive. Electrochemical characterization of Li_2S nanocrystals synthesized in this work demonstrate its potential for use in Li−S batteries and advanced LIBs, outperforming commercial Li_2S micropowders, in terms of (dis)charge capacity, cycling stability, output voltage, and voltage efficiency.

2. EXPERIMENTAL SECTION

2.1. Chemicals. Lithium (Li) grains (ACS reagent, stick dry), naphthalene (NAP, $C_{10}H_8$, 99%), anhydrous 1,2-dimethoxyethane (DME, $CH_3OCH_2CH_2OCH_3$, 99.5%), hexanes (ACS grade), lithium ribbon (99.9% trace metals basis, 0.38 mm), bis(trifluoromethane)-sulfonimide [LiTFSI, $(CF_3SO_2)_2NLi$, 99.95%], and tetra(ethylene glycol) dimethyl ether [TEGDME, $CH_3O(CH_2CH_2O)_4CH_3$, 99%] were purchased from Sigma-Aldrich. Lithium sulfide (Li_2S; 200 mesh, 99.9% metal basis) was purchased from Alfa Aesar. Anhydrous benzene-d_6 (C_6D_6, D-99.5%) was purchased from Cambridge Isotope Lab. Acetylene black (AB; 35−45 nm), anhydrous *N*-methylpyrrolidone (NMP, C_5H_9NO, >99.5%), poly(vinylidene fluoride) [PVDF, $-(C_2H_2F_2)_n-$, >99.5%], and copper foil (99.99%, 9 μm) were purchased from MTI Corp. AB and PVDF were dried in a vacuum oven at 60 °C for 24 h before use. All other chemicals were used as received.

2.2. Synthesis of Li_2S. The first step is to make the 0.04 M lithium naphthalenide (Li-NAP) solution in DME by adding Li grains and NAP powder at a molar ratio of Li:NAP = 1:1.3 into DME in an argon-protected glovebox. A total of 2 h of stirring produced a dark-green solution. After that, a Parr reactor (model 4793) was charged with 50 mL of the Li-NAP solution and connected to the H_2S stream (10% in argon). Figure S1 illustrates the schematic diagram and photograph of the apparatus. Initially, the H_2S/Ar mixture at a rate of 40 sccm flowed through a bypass line at ambient temperature and pressure to create a baseline reading. Afterward, the H_2S/Ar stream was switched to the Li-NAP solution. An online quadrupole mass spectrometer (QMS; Stanford Research Systems RGA300) was employed to analyze the effluent. The molar ratio between Li-NAP and H_2S consumed was controlled by the H_2S-flowing duration.

Subsequently, in the glovebox, centrifugation was employed to separate the solid product out of the reaction solution. The collected solid powder was washed with DME a few times before being dried for further analysis. The production yield of Li_2S on the basis of lithium was about 95.6%, which was very satisfactory considering some loss of sample in the solution. The liquid phase was taken out of the glovebox and then concentrated via rotary evaporation to $^1/_5$ of the original volume. The collected solution was kept in the glovebox for further analysis.

2.3. Product Characterization. X-ray diffraction (XRD) patterns were collected on a Philips X'Pert X-ray diffractometer using Cu Kα radiation (λ = 0.15405 nm). The sample was prepared in a glovebox by pressing the solid product into a thin film on a glass substrate. To avoid harmful reactions due to unavoidable air exposure during measurements, the solid was immediately covered with a drop of dried mineral oil in the glovebox. The background contribution from mineral oil was subtracted and corrected. Scanning electron microscopy (SEM) images were taken on a field-emission scanning electron micrometer (JEOL JSM-7000F). The sample was prepared by immobilizing the obtained Li_2S powder on an aluminum stub using double-sided carbon tape. The accelerating voltage was 5 kV. Thermogravimetric analysis (TGA) was performed using a Q50 thermogravimetric analyzer (TA Instruments). The sample was prepared by pressing Li_2S powders into pellet inside an argon-filled glovebox. Before each run, the sample holder (an alumina pan) was cleaned by heating the furnace under air to 800 °C for 15 min. To eliminate the influence of physisorbed gases during sample preparation, samples were also preheated at 50 °C for 30 min before collecting the valid TGA data. The nitrogen flow rate for the balance compartment and the argon flow rate for the sample compartment

DOI: 10.1021/acsami.5b09367
ACS Appl. Mater. Interfaces 2015, 7, 28444−28451

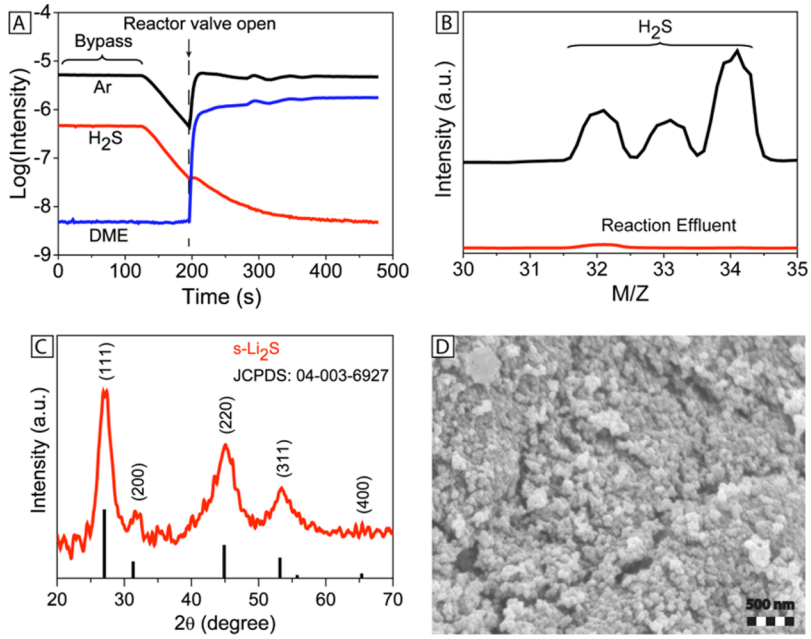

Figure 1. Characterization of the reaction for synthesizing Li_2S nanocrystals. (A) Time evolution of QMS to monitor the concentrations of key species in the gas phase: argon (black); H_2S (red); DME (blue). (B) MS spectra in the window of m/z 30−35 for the gaseous effluents through the bypass (black) and through the reactor (red). (C) XRD pattern of the obtained solid product (red) together with the stick pattern (black) of the Li_2S standard (JCPDS 04-003-6927). (D) SEM image of the obtained solid product.

were 40 and 60 mL/min, respectively. The temperature ramp rate was 2 °C/min.

The composition of the liquid supernatant produced by the reaction was analyzed by ^{1}H NMR (JEOL ECA-500) and gas chromatography−mass spectrometry (GC−MS). For NMR, 0.3 mL of the sample solution was dissolved in 0.2 mL of benzene-d_6 and loaded in a quartz sample tube. GC−MS analysis was conducted on a Varian CP-3800 gas chromatograph coupled to a Varian 1200 L quadrupole mass spectrometer, for which the solid phase in the separation column is 5% diphenylpolysiloxane and 5% dimethylpolysiloxane. The precondition of the column was accomplished by injecting pure solvent DME at 320 °C. After that, the sample analysis was performed by injecting 1 μL of the sample solution with the column temperature at 250 °C. In both cases, the flow rates of the carrier gas of helium were 1.3 mL/min.

2.4. Electrode Fabrication and Electrochemical Analyses. Swagelok cell electrodes were fabricated to assess the electrochemical properties of the synthesized Li_2S. Electrode fabrication began by first drying the as-synthesized Li_2S powder under argon in a tube furnace at 250 °C for 20 h to completely remove DME and NAP used in the synthesis. After that, the dried Li_2S (40 wt %), AB (45 wt %), and PVDF binder (15 wt %) were blended manually in a mortar. The resultant mixture was dispersed in a small amount of NMP and stirred overnight. Next, the obtained slurry was bladed onto a carbon paper (AvCarbP50) collector and dried at 110 °C for 6 h. Then, the electrodes were cut into small disks of 10 mm diameter using a compact precision disk cutter (MTI Corp., MSK-T-07). The mass loading of Li_2S was around 1.0 mg/cm^2. For benchmarking purposes, identical procedures were used to fabricate electrodes employing commercial Li_2S micropowders. Last, the half-cell batteries were assembled by using a lithium ribbon as the anode, a polypropylene membrane (Celgard 2500) as the separator, and 1.0 M LiTFSI in TEGDME as the electrolyte. Cyclic voltammograms (CVs) were collected on a potentiostat (Princeton Applied Research, Versastat 4). The cycling stability was assessed via the galvanostatic technique at 0.1 C (1 C = 1166 mA/g) by using an eight-channel battery analyzer (MTI Corp., BST8-MA). The specific capacity was calculated according to the mass of Li_2S.

3. RESULTS AND DISCUSSION

3.1. Demonstration of the Synthetic Method. On the basis of our previous work of abating H_2S with sodium naphthalenide (Na-NAP),[35] the Li_2S synthesis reaction is expected to be eq 4 and will be verified step by step.

$$2LiC_{10}H_8 + H_2S \rightarrow Li_2S + C_{10}H_{10} + C_{10}H_8 \quad (4)$$

Figure 1A plots the time evolution of the signal intensities from the carrier gas argon (black), the solvent DME (blue), and the reactant H_2S (red) recorded by the online QMS, for a typical reaction using the stoichiometric molar ratio of Li-NAP:H_2S = 2:1. Initially, the H_2S/Ar mixture flowed through a bypass line to establish a baseline reading. When the bypass was closed at t = 127 s, both argon and H_2S fall exponentially with a time constant characteristic of the gas dynamics of the sampling apparatus. At t = 195 s, the inlet and outlet valves of the reactor were opened simultaneously, and the argon signal immediately returns to its original value, accompanied by a step change in the signals associated with the volatile DME solvent. In stark contrast, the H_2S signal continues to exponentially decay, eventually dropping below the instrument's detection limit. This indicates that the H_2S supplied has been consumed at least 99.9%. The mass spectrum recorded from the effluent (Figure 1B, red) shows no signals of H_2S across the mass/charge (m/z) range of 32−34, while that recorded from the bypass mode (Figure 1B, black) shows the expected signals of H_2S evidently. Thus, the consumption of H_2S through its reaction with Li-NAP is demonstrated to be spontaneous, complete, and nearly instantaneous, as previously observed for the Na-NAP system.[35]

As shown in Figure 1C (red), the XRD pattern of the obtained solid product is well consistent with that of the Li_2S standard (black), indicating the successful generation of anhydrous, phase-pure, crystalline Li_2S. According to the Scherrer equation, which correlates crystalline domains with the peak width, Li_2S crystals are ∼5 nm in diameter.[36] The

DOI: 10.1021/acsami.5b09367
ACS Appl. Mater. Interfaces 2015, 7, 28444−28451

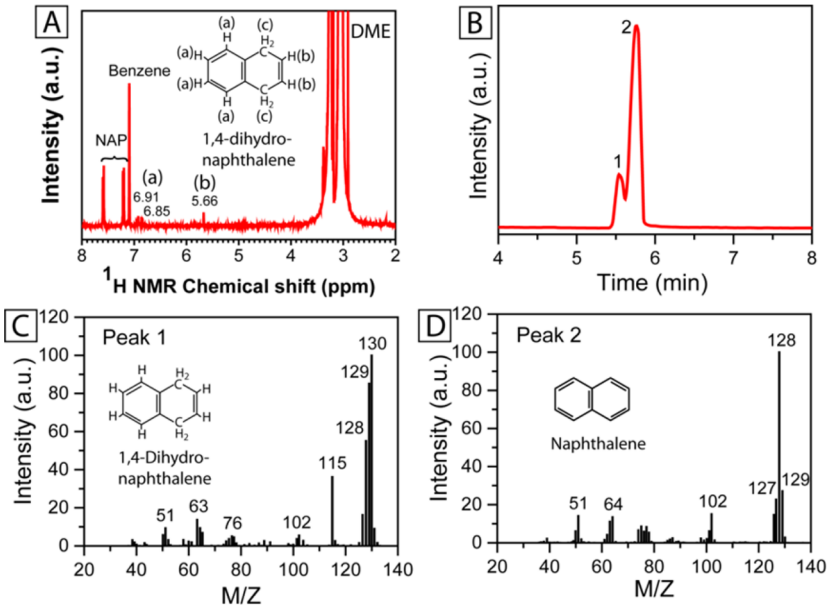

Figure 2. Characterization of the liquid phase collected from the synthetic reaction: (A) ^{1}H NMR spectrum; (B) gas chromatogram; (C) MS spectrum of peak 1 in part B; (D) MS spectrum of peak 2 in part B.

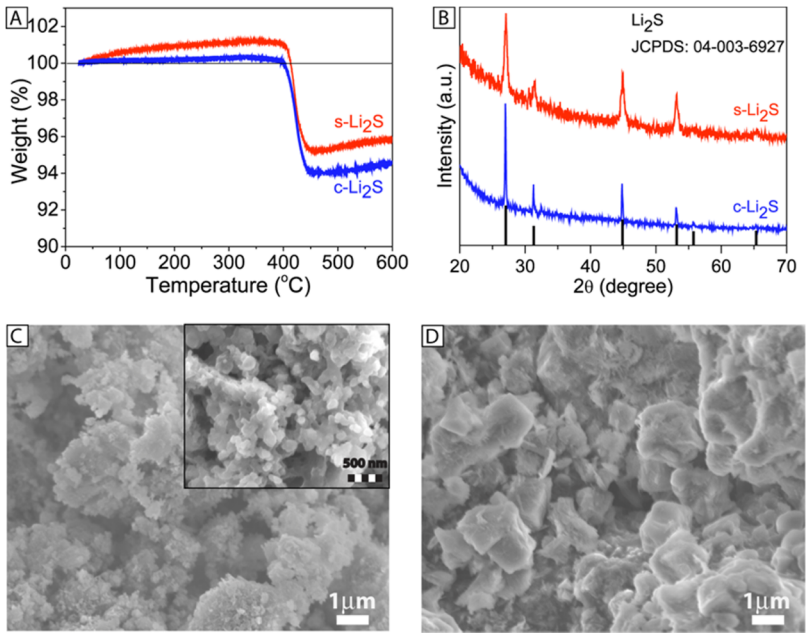

Figure 3. Characterization of s-Li_2S (red) after being dried at 250 °C for 20 h prior to electrochemical analyses, with c-Li_2S (blue) as a reference: (A) TGA plots; (B) XRD patterns; (C) SEM image of s-Li_2S; (D) SEM image of c-Li_2S.

SEM image (Figure 1D) shows that Li_2S nanocrystals aggregate as secondary particles of ~100 nm.

The ^{1}H NMR spectrum of the liquid phase, obtained by using benzene-d_6 as the solvent, is shown in Figure 2A. Besides the expected benzene, DME, and NAP,[37] three peaks at 6.91−5.66 ppm are assigned to the hydrogen atoms at positions a and b of 1,4-dihydronaphthalene.[38] The signal of the hydrogen atoms at position c is expected to show up at 3.3−2.9 ppm but is masked by the intense signal of DME. The chromatogram recorded by GC−MS (Figure 2B) shows two peaks. The corresponding MS spectra can be indexed to 1,4-dihydronaphthalene and NAP, respectively.[39,40] Thus, the characterization results shown in Figures 1 and 2 prove that the Li_2S synthesis follows eq 4, as previously observed for the Na-NAP system.[35]

Note that this synthetic method enables facile operation/separation because the reactants and products exist in different phases.

Then, we tested the effect of the molar ratio of Li-NAP/H_2S on the Li_2S synthesis (Figure S2). At the ratios of 3:1 and 1.5:1, the solid products were also phase pure anhydrous Li_2S nanocrystals with comparable sizes and shapes as in the case of the stoichiometric 2:1. Differently, in the case of 1:1, which was expected to produce LiHS, no solid product was observed in the reaction system. After evaporation of the solvent, only a gel-like substance was obtained, showing no sign of crystals. ^{1}H NMR did not produce any meaningful signals that could be assigned to known compounds. We believe that this is because LiHS fully dissolves in DME and exists in some unknown

DOI: 10.1021/acsami.5b09367
ACS Appl. Mater. Interfaces 2015, 7, 28444−28451

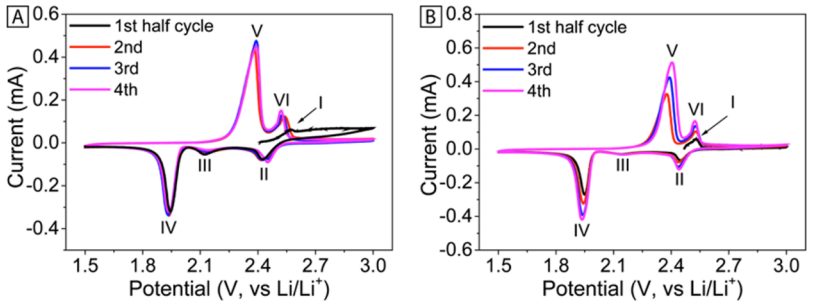

Figure 4. Typical CVs in the first four cycles of s-Li_2S (A) and c-Li_2S (B), where the scan rate is 0.1 mV/s.

complex form. For example, it is known that LiHS cannot precipitate out of ethanol but forms a LiHS/ethanol complex.[41] The comparison with our previous work indicates that LiHS has higher solubility/complexity in DME than NaHS.[35] These results demonstrate the robustness of this synthetic method to produce phase-pure Li_2S nanocrystals, and for practical operation, the use of a stoichiometric mixture is ideal to fully consume H_2S while maximizing the conversion of lithium to Li_2S.

3.2. Structural and Electrochemical Analyses. The synthesized Li_2S nanocrystals (denoted as s-Li_2S) were further characterized after drying to remove residual organics. The TGA plots in Figure 3A show that s-Li_2S (red) has a purity comparable to that of the commercial Li_2S micropowders (denoted as c-Li_2S, blue), as indicated by their nearly identical weight-loss profiles, of which the overall difference is only 1%. We speculate that the abrupt weight loss at about 400 °C is likely to result from the decomposition of some unknown impurities because the melting point of pure Li_2S is above 900 °C.[19] Possible culprits include lithium hydroxide (LiOH), hydrogen sulfide (H_2S), and lithium carbonate (Li_2CO_3),[16,42] which could be formed via the reaction between trace amounts of H_2O and CO_2 with Li_2S during sample storage and handling in the glovebox and environment.[43] The slight weight increase before 400 °C may be ascribed to the reaction of Li_2S with trace amounts of H_2O, O_2, and/or CO_2 in the carrier gas, which results in a greater reaction in the case of s-Li_2S due to its larger surface/volume ratio than c-Li_2S. XRD patterns in Figure 3B indicate a slight growth of the crystalline sizes for s-Li_2S from the original 5 nm to the present 20 nm after heat treatment, according to the Scherrer equation, but still much smaller than that of c-Li_2S (50 nm). Note that the estimated crystalline sizes denoted here provide a lower bound and are primarily used as a relative comparison among the different Li_2S materials because use of the Scherrer equation assumes that the nanosize effect is the only (or predominant) factor in peak broadening.[44] The crystal growth of s-Li_2S during annealing is also corroborated by the SEM image in Figure 3C, which includes more secondary particles without clear boundaries among nanocrystals. In contrast, c-Li_2S exists mainly as irregular microparticles of about 1−5 μm diameter with some smaller particles of about 100 nm, as shown in Figure 3D.

The electrochemical properties of both s-Li_2S and c-Li_2S were examined in half-cells according to the slurry protocol described in the Experimental Section. Parts A and B of Figure 4 show the first four cycles of the CVs of s-Li_2S and c-Li_2S, respectively. The observed results are consistent with the typical behavior of Li−S batteries reported in the literature.[32,45] As is widely known, the material's speciation cycles between two extreme states of sulfur (S_8) at 1.5 V and Li_2S at 3.0 V through reactions (5)−(9).[8,11]

$$2Li^+ + 2e^- + S_8 \leftrightarrow Li_2S_8 \quad (5)$$

$$2Li^+ + 2e^- + 3Li_2S_8 \leftrightarrow 4Li_2S_6 \quad (6)$$

$$2Li^+ + 2e^- + 2Li_2S_6 \leftrightarrow 3Li_2S_4 \quad (7)$$

$$2Li^+ + 2e^- + Li_2S_4 \leftrightarrow 2Li_2S_2 \quad (8)$$

$$2Li^+ + 2e^- + Li_2S_2 \leftrightarrow 2Li_2S \quad (9)$$

In the case of s-Li_2S, the initial open-circuit potential (OCP; 2.40 V vs Li/Li^+) that lies between 3.0 and 1.5 V can be ascribed to self-delithiation of Li_2S to lithiate the carbon additive, whose OCP is about 2.9 V.[46] In the first half-cycle, the anodic current with a weak peak at 2.57 V (peak I) corresponds to delithiation of Li_2S to form sulfur.[11,24] In the subsequent cathodic scans, three characteristic peaks are observed at ca. 2.44 V (peak II, strong), ca. 2.12 V (peak III, weak), and 1.94 V (peak IV, very strong), respectively.[11,24] Peak II is typically assigned to the reduction of S_8 to polysulfides (Li_2S_n, where n = 4−8) in three steps (eqs 5−7). Peak III is believed to result from the reduction of Li_2S_4 to insoluble Li_2S_2 (eq 8).[11] Peak IV is due to the conversion of Li_2S_2 to Li_2S (eq 9).[11] In contrast, the subsequent anodic scans only have two distinguishable peaks at 2.39 V (peak V) and 2.53 V (peak VI), which correspond to the oxidation of Li_2S first to polysulfides and subsequently to S_8, respectively. The steady peak potentials and current intensities during the illustrated cycles in Figure 4A manifest the good stability and reversibility of the s-Li_2S electrode. The electrochemistry of the commercial c-Li_2S is quite similar because the six peaks just described are readily identified (Figure 4B). The prominent difference between the two materials is their stability. In the case of c-Li_2S, the anodic (cathodic) peaks shift more positive (negative) and the current intensities consecutively increase over the first few cycles, indicating the inferiority of c-Li_2S to s-Li_2S in electrolyte wettability and electrochemical reversibility.[47]

The galvanostatic technique was employed to assess the cycling stabilities (Figure 5) of s-Li_2S (red) and c-Li_2S (blue) electrodes in both the charge (solid circles and squares) and discharge (open circles and squares) processes. s-Li_2S is superior to c-Li_2S in all regards. The initial charge (delithiation) and discharge (lithiation) capacities for s-Li_2S are 724 and 669 mAh/g, respectively, which compare well with the theoretical limit of 1166 mAh/g considering that electrode fabrication was not optimized.[4] The performance gradually declines, and the half-life, defined as the cycles spent to reach 50% of the initial charge capacity, is 45 cycles for s-Li_2S. Because Li_2S is in the

DOI: 10.1021/acsami.5b09367
ACS Appl. Mater. Interfaces 2015, 7, 28444−28451

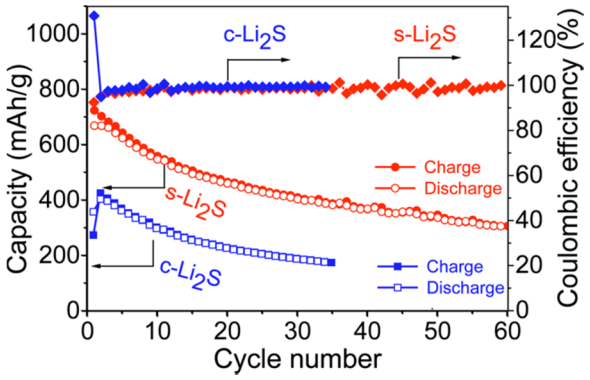

Figure 5. Typical plots of the specific capacity in charge (solid circles and squares) and discharge (open circles and squares) processes and CE (solid diamonds) versus cycle number for both s-Li_2S (red) and c-Li_2S (blue), for which the galvanostatic current is 116.6 mA/g (0.1 C, where 1 C = 1166 mA/g).

fully lithiated state, the Coulombic efficiency (CE) is defined as the ratio of lithiation (discharge) capacity to the delithiation (charge) capacity.[48] The s-Li_2S displayed 92% CE in the first cycle and then quickly increased to 98−100% in all subsequent cycles.

In contrast, the initial charge capacity of the c-Li_2S is only 272 mAh/g. The subsequent discharge capacity contributes 356 mAh/g, resulting in a "abnormally" high CE (CE = 356/272 = 131%), which may be ascribed to the compensation for the loss of Li due to self-delithiation before the measurement and the dissolution of polysulfides during the discharge process, as pointed out in the literature.[49−51] In the second cycle, the charge capacity bounces to 424 mAh/g. The CE values in the subsequent cycles are comparable with those of s-Li_2S. The stability c-Li_2S declines in a similar fashion but reaches its half-life after only 23 cycles. The differences in the initial CE and stability suggest that s-Li_2S particles, compared with c-Li_2S particles, are better protected by the additives used in electrode fabrication because of their smaller particle sizes. Moreover, s-Li_2S herein also performs significantly better than c-Li_2S in the literature (630 mAh/g for the initial capacity and 240 mAh/g at the 30th cycle).[9]

Despite no optimization of the electrode fabrication procedure, the performance of s-Li_2S synthesized in this work compares favorably with some s-Li_2S particles in the literature. For instance, the Li_2S−C nanocomposite made by reacting lithium sulfate with resorcinol/formaldehyde showed an initial capacity of 350 mAh/g and 300 mAh/g at the 30th cycle;[32] the Li_2S−C nanocomposite made by thermally annealing a mixture of polysufilde Li_2S_3 and polyacrylonitrile exhibited specific capacities of 500 mAh/g initially and 500 mAh/g at the 20th cycle;[27] the Li_2S−C nanocomposite made by ball-milling Li_2S micropowder and carbon precursor presented the specific capacity of 560 mAh/g initially and 420 mAh/g at the 30th cycle.[52] s-Li_2S synthesized in this work displays a significantly higher initial (dis)charge capacity but inferior cycling stability. It is expected that the latter issue can be addressed through the optimization of electrode fabrication procedures, by following published strategies in the literature,[4,9,12,26,53−56] a topic of our future work.

As shown in Figure 6, s-Li_2S and c-Li_2S present different potential profiles in the first half-cycle (black). With respect to s-Li_2S, as highlighted by the inset of Figure 6A, a small potential barrier between 2.46 and 2.52 V is overcome to contribute the initial delithiation capacity of 50 mAh/g. After that, only one plateau at 2.42 V is observed to contribute the remaining 670 mAh/g before sharply rising to the cutoff potential 3.0 V. In contrast, the potential profile of c-Li_2S (Figure 6B, black) exhibits a flat plateau at 2.50 V for the initial 200 mAh/g and a sloping plateau between 2.8 and 3.0 V for the remaining 70 mAh/g. The first plateau can be considered to be a consequence of encountering a continuous potential barrier.

The potential profile of s-Li_2S described above confirms that this material does not require a significant potential to activate its charge capacity, consistent with literature reports for Li_2S nanoparticles.[4,12,15,24,26,57] However, Li_2S micropowders reported in the literature require one to overcome a large activation barrier in the range of 3.5 and 4.0 V.[9] The activation process contributes only 48 mAh/g, while the subsequent plateau at 2.5 V can contribute as high as 600 mAh/g.[9] Thus, our c-Li_2S electrode seems to behave partially like Li_2S nanoparticles and partially like Li_2S microparticles. When referring to our XRD result (which shows the crystalline sizes of c-Li_2S to be ≥50 nm) and SEM observation (some particles are around 100 nm) in Figure 3, we speculate that the capacity observed in the c-Li_2S electrode be predominantly from those nano/submicroparticles; microparticles seem barely activated because of the requirement of higher cutoff potentials.

The potential profiles in the subsequent cycles corroborate the lithiation/deliathiation mechanism described in the discussion of the cyclic voltammetry results (Figure 4). Both s-Li_2S and c-Li_2S show three distinguishable plateaus during the discharge processes and two plateaus during the charge processes. For s-Li_2S (Figure 6A), the discharge plateaus are at 2.45 V (eqs 5−7), 2.2 V (eq 8), and 2.06 V (eq 9); the charge plateaus are at 2.25 V (eqs 8 and 9) and 2.50 V (eqs 5−7). All of these values except 2.06 and 2.25 V are essentially

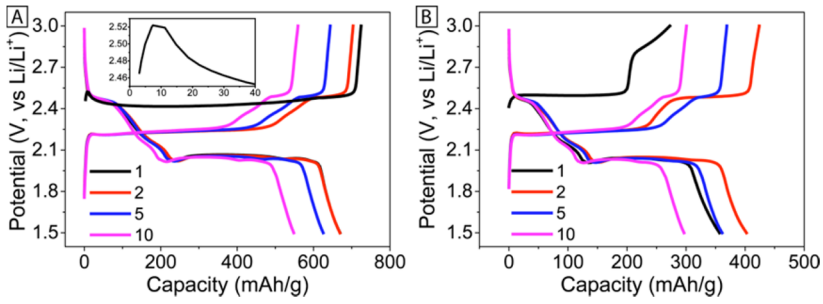

Figure 6. Several cycles of voltage profiles against the specific capacities for s-Li_2S (A) and c-Li_2S (B), where the inset in part A highlights the activation period in the first cycle.

DOI: 10.1021/acsami.5b09367
ACS Appl. Mater. Interfaces 2015, 7, 28444−28451

consistent with the corresponding peak potentials in the CV (Figure 4A). The small differences in the positions of these two peak potentials between the galvanostatic and cyclic voltammetric processes (2.06 V vs 1.94 V and 2.25 V vs 2.39 V) can be explained by the different reaction kinetics and polarization effects. In the case of c-Li_2S (Figure 6B), while the charge plateau (2.25 V) is the same as that of s-Li_2S, the discharge plateau (2.02 V) is slightly lower, which means that, in principle, s-Li_2S could provide higher energy and power densities than c-Li_2S. Moreover, it is worth noting that the potential hysteresis between the charge plateau (2.25 V) and the discharge plateau (2.06 V) for the s-Li_2S electrode herein is only 0.19 V (lower than 0.23 V for c-Li_2S), comparable with the smallest value reported in the literature (0.2 V),[12] where most values are in the range of 0.25−0.4 V.[4,9,11] Small hysteresis is desirable and indicative of high voltage efficiency.

The electrochemical analyses above show that the s-Li_2S nanocrystals synthesized from reacting H_2S with Li-NAP hold promise as electrode materials for advanced rechargeable batteries. They are superior to commercial c-Li_2S in (dis)charge capacity, cycling stability, output voltage, and voltage efficiency. Despite simple electrode fabrication procedures, their performance is already comparable with some s-Li_2S materials reported in the literature.

4. CONCLUSION

In conclusion, we have demonstrated a new method of synthesizing anhydrous Li_2S nanocrystals and confirmed their promise as potential cathode materials for Li−S batteries and advanced LIBs. The synthesis is realized by reacting Li-NAP with H_2S, a thermodynamically spontaneous reaction at ambient temperature and pressure that is fast, complete, and irreversible. Compared with the commercial Li_2S micropowders (1- 5 μm), the synthesized Li_2S nanocrystals (100 nm) present a superior performance in all regards, including the (dis)charge capacity, cycling stability, output voltage, and voltage efficiency. These results clearly manifest the potential of this synthetic method for practical production of high-quality Li_2S nanoparticles because it is conducted at mild conditions and Li_2S is the only solid phase, facilitating separation and purification. Work is in progress to improve the battery performance through optimization of electrode fabrication and by tuning the morphology of Li_2S nanocrystals through the judicious choice of alternative complexing reagents and solvents.

■ ASSOCIATED CONTENT

Supporting Information

The Supporting Information is available free of charge on the ACS Publications website at DOI: 10.1021/acsami.5b09367.

Schematic diagram and photograph of the apparatus as well as XRD patterns and SEM images of Li_2S produced by using different molar ratios of Li-NAP/H_2S (PDF)

■ AUTHOR INFORMATION

Corresponding Authors

*E-mail: cwolden@mines.edu.
*E-mail: yonyang@mines.edu.

Author Contributions

The manuscript was written through contributions of all authors. All authors have given approval to the final version of the manuscript.

Funding

This work is financially supported by the Startup Fund for Y.Y. from the Colorado School of Mines. C.A.W. acknowledges support by the National Science Foundation through Award DMR-1207294. C.B. acknowledges support by the Assistant Secretary for Energy Efficiency and Renewable Energy, Office of Vehicle Technologies of the U.S. Department of Energy under Contract No. DE-AC02-05CH11231, Subcontract No. DE-AC-36-08GO28308 under Exploratory Battery Materials Research program.

Notes

The authors declare no competing financial interest.

■ ACKNOWLEDGMENTS

We are thankful to Professor Yuan Yang for her helpful advice on NMR measurements.

■ REFERENCES

(1) Goodenough, J. B. Evolution of Strategies for Modern Rechargeable Batteries. *Acc. Chem. Res.* **2013**, *46*, 1053−1061.
(2) Whittingham, M. S. History, Evolution, and Future Status of Energy Storage. *Proc. IEEE* **2012**, *100*, 1518−1534.
(3) Tarascon, J. M.; Armand, M. Issues and Challenges Facing Rechargeable Lithium Batteries. *Nature* **2001**, *414*, 359−367.
(4) Wu, F.; Kim, H.; Magasinski, A.; Lee, J. T.; Lin, H.-T.; Yushin, G. Harnessing Steric Separation of Freshly Nucleated Li_2S Nanoparticles for Bottom-up Assembly of High-Performance Cathodes for Lithium-Sulfur and Lithium-Ion Batteries. *Adv. Energy Mater.* **2014**, *4*, 1400196.
(5) Bruce, P. G.; Freunberger, S. A.; Hardwick, L. J.; Tarascon, J. M. Li-O(2) and Li-S Batteries with High Energy Storage. *Nat. Mater.* **2012**, *11*, 19−29.
(6) Manthiram, A.; Fu, Y.; Su, Y.-S. Challenges and Prospects of Lithium-Sulfur Batteries. *Acc. Chem. Res.* **2013**, *46*, 1125−1134.
(7) Evers, S.; Nazar, L. F. New Approaches for High Energy Density Lithium-Sulfur Battery Cathodes. *Acc. Chem. Res.* **2013**, *46*, 1135−1143.
(8) Yin, Y. X.; Xin, S.; Guo, Y. G.; Wan, L. J. Lithium-Sulfur Batteries: Electrochemistry, Materials, and Prospects. *Angew. Chem., Int. Ed.* **2013**, *52*, 13186−13200.
(9) Yang, Y.; Zheng, G.; Misra, S.; Nelson, J.; Toney, M. F.; Cui, Y. High-Capacity Micrometer-Sized Li_2S Particles as Cathode Materials for Advanced Rechargeable Lithium-Ion Batteries. *J. Am. Chem. Soc.* **2012**, *134*, 15387−15394.
(10) Mikhaylik, Y.; Kovalev, I.; Schock, R.; Kumaresan, K.; Xu, J.; Affinito, J. High Energy Rechargeable Li-S Cells for EV Application. Status, Remaining Problems and Solutions. *ECS Trans.* **2010**, *25*, 23−34.
(11) Yang, Y.; Zheng, G. Y.; Cui, Y. Nanostructured Sulfur Cathodes. *Chem. Soc. Rev.* **2013**, *42*, 3018−3032.
(12) Yang, Y.; McDowell, M. T.; Jackson, A.; Cha, J. J.; Hong, S. S.; Cui, Y. New Nanostructured Li_2S/Silicon Rechargeable Battery with High Specific Energy. *Nano Lett.* **2010**, *10*, 1486−1491.
(13) Seh, Z. W.; Li, W. Y.; Cha, J. J.; Zheng, G. Y.; Yang, Y.; McDowell, M. T.; Hsu, P. C.; Cui, Y. Sulphur-TiO_2 Yolk-Shell Nanoarchitecture with Internal Void Space for Long-Cycle Lithium-Sulphur Batteries. *Nat. Commun.* **2013**, *4*, 1331.
(14) Zhou, W.; Yu, Y.; Chen, H.; DiSalvo, F. J.; Abruna, H. D. Yolk@Shell Structure of Polyaniline-Coated Sulfur for Lithium-Sulfur Batteries. *J. Am. Chem. Soc.* **2013**, *135*, 16736−16743.
(15) Zhang, K.; Wang, L.; Hu, Z.; Cheng, F.; Chen, J. Ultrasmall Li_2S Nanoparticles Anchored in Graphene Nanosheets for High-Energy Lithium-Ion Batteries. *Sci. Rep.* **2014**, *4*, 6467.
(16) Ikeda, N.; Yamamoto, K. Method of Manufacturing Lithium Sulfide. Patent EP0802159 B1, 2001.
(17) Miyashita, N. Method for Producing Lithium Sulfide for Lithium Ion Cell Solid Electrolyte Material. U.S. Patent 20140037535 A1, 2014.

DOI: 10.1021/acsami.5b09367
ACS Appl. Mater. Interfaces 2015, 7, 28444−28451

(18) Hofmann, A. F.; Fronczek, D. N.; Bessler, W. G. Mechanistic Modeling of Polysulfide Shuttle and Capacity Loss in Lithium-Sulfur Batteries. *J. Power Sources* **2014**, *259*, 300−310.
(19) Lide, D. R. *CRC Handbook of Chemistry and Physics*, 88th ed.; CRC Press, Taylor & Francis Group: New York, 2007−2008.
(20) Takeuchi, T.; Sakaebe, H.; Kageyama, H.; Senoh, H.; Sakai, T.; Tatsumi, K. Preparation of Electrochemically Active Lithium Sulfide-Carbon Composites using Spark-Plasma-Sintering Process. *J. Power Sources* **2010**, *195*, 2928−2934.
(21) Agostini, M.; Hassoun, J.; Liu, J.; Jeong, M.; Nara, H.; Momma, T.; Osaka, T.; Sun, Y. K.; Scrosati, B. A Lithium-Ion Sulfur Battery Based on a Carbon-Coated Lithium-Sulfide Cathode and an Electrodeposited Silicon-Based Anode. *ACS Appl. Mater. Interfaces* **2014**, *6*, 10924−10928.
(22) Hassoun, J.; Scrosati, B. A High-Performance Polymer Tin Sulfur Lithium Ion Battery. *Angew. Chem., Int. Ed.* **2010**, *49*, 2371−2374.
(23) Nagao, M.; Hayashi, A.; Tatsumisago, M. High-Capacity Li_2S-Nanocarbon Composite Electrode for All-Solid-State Rechargeable Lithium Batteries. *J. Mater. Chem.* **2012**, *22*, 10015−10020.
(24) Cai, K.; Song, M.-K. K.; Cairns, E. J.; Zhang, Y. Nanostructured Li_2S-C Composites as Cathode Material for High-energy Lithium/Sulfur Batteries. *Nano Lett.* **2012**, *12*, 6474−6479.
(25) Wu, F.; Magasinski, A.; Yushin, G. Nanoporous Li_2S and MWCNT-linked Li_2S powder cathodes for lithium-sulfur and lithium-ion battery chemistries. *J. Mater. Chem. A* **2014**, *2*, 6064−6070.
(26) Wang, C.; Wang, X.; Yang, Y.; Kushima, A.; Chen, J.; Huang, Y.; Li, J. Slurryless Li_2S/Reduced Graphene Oxide Cathode Paper for High-Performance Lithium Sulfur Battery. *Nano Lett.* **2015**, *15*, 1796−1802.
(27) Guo, J.; Yang, Z.; Yu, Y.; Abruña, H. D.; Archer, L. A. Lithium-Sulfur Battery Cathode Enabled by Lithium-Nitrile Interaction. *J. Am. Chem. Soc.* **2013**, *135*, 763−767.
(28) Han, K.; Shen, J. M.; Hayner, C. M.; Ye, H. Q.; Kung, M. C.; Kung, H. H. Li_2S-Reduced Graphene Oxide Nanocomposites as Cathode Material for Lithium Sulfur Batteries. *J. Power Sources* **2014**, *251*, 331−337.
(29) Hwa, Y.; Zhao, J.; Cairns, E. J. Lithium Sulfide (Li_2S)/Graphene Oxide Nanospheres with Conformal Carbon Coating as a High-Rate, Long-Life Cathode for Li/S Cells. *Nano Lett.* **2015**, *15*, 3479−3486.
(30) Lin, Z.; Liu, Z. C.; Dudney, N. J.; Liang, C. D. Lithium Superionic Sulfide Cathode for All-Solid Lithium-Sulfur Batteries. *ACS Nano* **2013**, *7*, 2829−2833.
(31) Zheng, S. Y.; Chen, Y.; Xu, Y. H.; Yi, F.; Zhu, Y. J.; Liu, Y. H.; Yang, J. H.; Wang, C. S. In Situ Formed Lithium Sulfide/Microporous Carbon Cathodes for Lithium-Ion Batteries. *ACS Nano* **2013**, *7*, 10995−11003.
(32) Yang, Z.; Guo, J.; Das, S. K.; Yu, Y.; Zhou, Z.; Abruna, H. D.; Archer, L. A. In situ Synthesis of Lithium Sulfide-Carbon Composites as Cathode Materials for Rechargeable Lithium Batteries. *J. Mater. Chem. A* **2013**, *1*, 1433−1440.
(33) Kohl, M.; Bruckner, J.; Bauer, I.; Althues, H.; Kaskel, S. Synthesis of Highly Electrochemically Active Li_2S Nanoparticles for Lithium-Sulfur-Batteries. *J. Mater. Chem. A* **2015**, *3*, 16307−16312.
(34) Meng, X. B.; Comstock, D. J.; Fister, T. T.; Elam, J. W. Vapor-Phase Atomic-Controllable Growth of Amorphous Li_2S for High-Performance Lithium-Sulfur Batteries. *ACS Nano* **2014**, *8*, 10963−10972.
(35) Li, X. M.; Morrish, R. M.; Yang, Y.; Wolden, C. A.; Yang, Y. Thermodynamically Favorable Conversion of Hydrogen Sulfide to Valuable Products through Reaction with Sodium Naphthalenide. *ChemPlusChem* **2015**, *80*, 1508−1512.
(36) Cloud, J. E.; Wang, Y.; Li, X.; Yoder, T. S.; Yang, Y.; Yang, Y. Lithium Silicide Nanocrystals: Synthesis, Chemical Stability, Thermal Stability, and Carbon Encapsulation. *Inorg. Chem.* **2014**, *53*, 11289−11297.
(37) Cheng, Y.; Fan, H. F.; Wu, S. X.; Wang, Q. A.; Guo, J.; Gao, L.; Zong, B. N.; Han, B. X. Enhancing the Selectivity of the Hydrogenation of Naphthalene to Tetralin by High Temperature Water. *Green Chem.* **2009**, *11*, 1061−1065.
(38) Japan National Institute of Advanced Industrial Science and Technology (AIST). Spectral Database for Organic Compounds, S.D.B.S.
(39) Tsimeli, K.; Triantis, T. M.; Dimotikali, D.; Hiskia, A. Development of a Rapid and Sensitive Method for the Simultaneous Determination of 1,2-Dibromoethane, 1,4-Dichlorobenzene and Naphthalene Residues in Honey Using HS-SPME Coupled with GC-MS. *Anal. Chim. Acta* **2008**, *617*, 64−71.
(40) NIST-MS-Search, NIST14, and Wiley databases, 2014.
(41) Jones, J. H.; Thomas, J. S. CCCLXXXIX.-The Action of Hydrogen Sulphide on Lithium Ethoxide. Lithium Hydrosulphide. *J. Chem. Soc., Trans.* **1923**, *123*, 3285−3294.
(42) Verma, N. K.; Khanna, S. K.; Kapila, B. *Comprehensive Chemistry XI*; Laxmi Publications: New Delhi, India, 2010; Chapter 10.
(43) Zhao, J.; Lu, Z.; Wang, H.; Liu, W.; Lee, H.-W.; Yan, K.; Zhuo, D.; Lin, D.; Liu, N.; Cui, Y. Artificial Solid Electrolyte Interphase-Protected Li_xSi Nanoparticles: An Efficient and Stable Prelithiation Reagent for Lithium-Ion Batteries. *J. Am. Chem. Soc.* **2015**, *137*, 8372−8375.
(44) Patterson, A. The Scherrer Formula for X-Ray Particle Size Determination. *Phys. Rev.* **1939**, *56*, 978−982.
(45) Fu, Y.; Su, Y.-S.; Manthiram, A. Li_2S-Carbon Sandwiched Electrodes with Superior Performance for Lithium-Sulfur Batteries. *Adv. Energy Mater.* **2014**, *4*, 1300655.
(46) Zhao, M. C.; Xu, M. M.; Dewald, H. D.; Staniewicz, R. J. Open-Circuit Voltage Study of Graphite-Coated Copper Foil Electrodes in Lithium-Ion Battery Electrolytes. *J. Electrochem. Soc.* **2003**, *150*, A117−A120.
(47) Zheng, J.; Lv, D.; Gu, M.; Wang, C.; Zhang, J.-G.; Liu, J.; Xiao, J. How to Obtain Reproducible Results for Lithium Sulfur Batteries? *J. Electrochem. Soc.* **2013**, *160*, A2288−A2292.
(48) Jayaprakash, N.; Shen, J.; Moganty, S. S.; Corona, A.; Archer, L. A. Porous Hollow Carbon@Sulfur Composites for High-Power Lithium-Sulfur Batteries. *Angew. Chem., Int. Ed.* **2011**, *50*, 5904−5908.
(49) Xin, S.; Gu, L.; Zhao, N. H.; Yin, Y. X.; Zhou, L. J.; Guo, Y. G.; Wan, L. J. Smaller Sulfur Molecules Promise Better Lithium-Sulfur Batteries. *J. Am. Chem. Soc.* **2012**, *134*, 18510−18513.
(50) Zhang, B.; Qin, X.; Li, G. R.; Gao, X. P. Enhancement of long stability of sulfur cathode by encapsulating sulfur into micropores of carbon spheres. *Energy Environ. Sci.* **2010**, *3*, 1531−1537.
(51) Xi, K.; Kidambi, P. R.; Chen, R.; Gao, C.; Peng, X.; Ducati, C.; Hofmann, S.; Kumar, R. V. Binder free three-dimensional sulphur/few-layer graphene foam cathode with enhanced high-rate capability for rechargeable lithium sulphur batteries. *Nanoscale* **2014**, *6*, 5746−5753.
(52) Jeong, S.; Bresser, D.; Buchholz, D.; Winter, M.; Passerini, S. Carbon Coated Lithium Sulfide Particles for Lithium Battery Cathodes. *J. Power Sources* **2013**, *235*, 220−225.
(53) Shin, J. H.; Cairns, E. J. N-Methyl-(n-butyl)pyrrolidinium bis(trifluoromethanesulfonyl)imide-LiTFSI-poly(ethylene glycol) dimethyl ether mixture as a Li/S cell electrolyte. *J. Power Sources* **2008**, *177*, 537−545.
(54) Su, Y. S.; Manthiram, A. Lithium-Sulphur Batteries with a Microporous Carbon Paper as a Bifunctional Interlayer. *Nat. Commun.* **2012**, *3*, 1166.
(55) Chung, S.-H.; Manthiram, A. A Hierarchical Carbonized Paper with Controllable Thickness as a Modulable Interlayer System for High Performance Li-S Batteries. *Chem. Commun.* **2014**, *50*, 4184−4187.
(56) Balach, J.; Jaumann, T.; Klose, M.; Oswald, S.; Eckert, J.; Giebeler, L. Mesoporous Carbon Interlayers with Tailored Pore Volume as Polysulfide Reservoir for High-Energy Lithium-Sulfur Batteries. *J. Phys. Chem. C* **2015**, *119*, 4580−4587.
(57) Ye, F. M.; Hou, Y.; Liu, M. N.; Li, W. F.; Yang, X. W.; Qiu, Y. C.; Zhou, L. S.; Li, H. F.; Xu, Y. J.; Zhang, Y. G. Fabrication of Mesoporous Li_2S-C Nanofibers for High Performance Li/Li_2S Cell Cathodes. *Nanoscale* **2015**, *7*, 9472−9476.

DOI: 10.1021/acsami.5b09367
ACS Appl. Mater. Interfaces 2015, 7, 28444−28451